Measurement of the 671-nm tune-out wavelength of 7 Li by atom interferometry

Boris Decamps, Jacques Vigué, Alexandre Gauguet, Matthias Büchner

Measurement of the 671-nm tune-out wavelength of ^{7}Li by atom interferometry

B. Décamps, J. Vigué, A. Gauguet, and M. Büchner*
Laboratoire Collisions Agrégats Réactivité–IRSAMC Université Toulouse III Paul Sabatier, CNRS UMR 5589, Toulouse, France

(Received 17 December 2019; accepted 29 January 2020; published 18 March 2020)

We have measured the tune-out wavelength of lithium isotope ^{7}Li at 671 nm. We have used our atom interferometer to measure the phase shift due to the dynamical Stark effect as a function of the laser frequency when a laser beam was focused on a single interferometer arm. The tune-out wavelength is a function of the hyperfine F, m_F sublevel, and we have prepared the atoms in the sublevel $F = 2, m_F = +2$ or -2. We find that the tune-out frequency of the $F = 2, m_F = +2$ sublevel is at 3388(8) MHz to the blue of the $^2S_{1/2}$, $F = 1 \rightarrow {}^2P_{1/2}, F' = 2$ transition, the accuracy of this measurement being limited by imperfect optical pumping. This measurement is in excellent agreement with its theoretical value, and, once corrected for different tensorial contributions, our measurement agrees with the more precise measurement of Copenhaver *et al.* [Phys. Rev. A **100**, 063603 (2019)], who also used atom interferometry but different experimental conditions.

DOI: 10.1103/PhysRevA.101.033614

I. INTRODUCTION

Atom interferometry has developed rapidly since 1991, and many very interesting results have thus been obtained, which are described in books or review papers [1–3]. Atom interferometry demonstrates an extreme sensitivity for the measurement of acceleration: such a variation is detected through the phase shift of the interferometer fringe signal.

In this paper we consider the measurement of the atom electric polarizability. This quantity cannot be measured by spectroscopy, which has access only to the difference of the polarizabilities of two internal states. If we except macroscopic techniques based on the dielectric constant or the index of refraction, which have been applied mostly to noble gases, all the polarizability measurements rely on mechanical effects; the traditional technique due to Scheffers and Stark [4] in 1934 is the deflection of the atom (or molecule) trajectory by an electric field gradient [5,6].

Atom interferometry was first applied in 1995 to the high-precision measurement of the static polarizability of the sodium atom by Ekstrom *et al.* [7] (see also [8]) and of the lithium atom by our research group in 2005 [9,10]. The dynamical polarizability of the rubidium atom was measured in 2008 by Deissler *et al.* [11] using a guided wave atom interferometer. Since 2010, the research group of Cronin has developed high-precision measurements of the absolute values and the ratios of the static polarizability of Na, K, Rb, and Cs [12–14].

There is great interest in the dynamical polarizability, also called the AC Stark effect or light shift, because it is an efficient tool to manipulate cold atoms. When an atom interacts with an electric field $\mathbf{E}(\mathbf{r})$ of frequency ω, at second-order perturbation expansion, the energy of the internal state i is modified by the quantity U_i given by

$$U_i(\mathbf{r}) \approx -\alpha_i(\omega)\mathbf{E}^2(\mathbf{r})/2, \tag{1}$$

where $\alpha_i(\omega)$ is the atom dynamical polarizability of state i. This expression of $U_i(\mathbf{r})$, which is the lowest nonvanishing contribution, is proportional to $\mathbf{E}^2(\mathbf{r})$, i.e., to the local light intensity, and it depends on the state i, on the light polarization, and on the frequency ω. The polarizability $\alpha_i(\omega)$ cancels for certain frequencies, and the corresponding wavelengths are called tune-out wavelengths. (These wavelengths have also been called magic-zero wavelengths in some papers; they should not be confused with magic wavelengths, for which the difference of the polarizabilities of two internal states vanishes.) In the case of the ground state, the existence of such frequencies can be explained by a very simple argument: when the light frequency ω crosses the frequency ω_0 of a resonance transition, the contribution of this transition, which is resonantly enhanced and positive when $\omega < \omega_0$, becomes negative when $\omega > \omega_0$. As a consequence, a tune-out frequency is expected between two resonances and, in particular, in the case of alkali atoms, between the fine-structure components of their D lines.

The tune-out wavelengths are particularly interesting for two main reasons. From the point of view of applications, this property can be used to selectively apply a potential on an atomic (or isotopic) species and not on another one [15–17]. Early applications of this idea can be found in Refs. [18,19].

From a theoretical point of view, it is possible to accurately calculate tune-out wavelengths, and they can also be measured with great accuracy because their measurement does not require the calibration of the light intensity, which is needed for measurement of the polarizability itself. The comparison of calculations and measurements provides accurate tests of the calculations, and they give access to very precise information on oscillator strengths [20].

Here we describe our measurement of the tune-out wavelength of the ^{7}Li atom, near 671 nm, between the two components of the D line, using our thermal atom interferometer. Copenhaver *et al.* [22] have used a cold lithium atom interferometer to measure the same tune-out wavelength. The two experiments differ on some important aspects, and we will compare their results to ours.

*matthias.buchner@irsamc.ups-tlse.fr

TABLE I. This table presents measurements of the tune-out wavelengths. For each measurement, we give the atom, an approximate value of the tune-out wavelength λ_{TO}, the experimental technique used (with the following short-hand: OMMT for optical modulation of a magnetic trap, AI for atom interferometry, AD for atom diffraction, PP for pump and probe), and their references.

Atom	λ_{TO}	Experiment	References
He^*	413 nm	OMMT	[21]
Lithium	671 nm	AI	[22]
Potassium	769 nm	AI	[23–25]
Rubidium	790 nm	AI	[26]
Rubidium	790 nm	AD	[27]
Rubidium	790 nm	PP	[28]
Rubidium	421,423 nm	AD	[29]
Dysprosium	741 nm	AD	[30]

The content of our paper is organized as follows: Section II recalls the previous knowledge on tune-out wavelengths; Sec. III presents a theoretical overview and its application to the case of lithium; Sec. IV describes our experimental setup; and in Sec. V we present our measurement of the Stark phase shift and the tune-out frequency, which is discussed and compared to the measurement of Copenhaver *et al.* [22]. A brief conclusion in Sec. VI and an Appendix complete our paper.

II. PREVIOUS MEASUREMENTS AND CALCULATIONS OF TUNE-OUT WAVELENGTHS

The measurements of tune-out wavelengths have been made by various techniques and on different atoms. We have collected to the best of our knowledge the measurements in Table I. There are also many calculations of tune-out wavelengths and, frequently, several tune-out wavelengths are calculated in the same paper. The calculation of the 413-nm tune-out wavelength for He^* has been made by several research groups [31,32] and in some works with very sophisticated methods [33–35]. Many works have been devoted to the alkali atoms: lithium [17,36], including a calculation with Hylleraas wave functions [37], sodium [17], potassium [17,38], rubidium [17,26,27,29], cesium [17], and francium [39,40]. Other atoms have also been considered, e.g., alkaline-earth-metal atoms [20,41].

III. THEORETICAL OVERVIEW AND APPLICATION TO THE LITHIUM 671 NM TUNE-OUT WAVELENGTH

A. Interaction of an atom with an electromagnetic wave

An atom interacts with a plane electromagnetic wave of wave vector $\mathbf{k}$, angular frequency ω, and polarization vector ϵ, with an electric field given by $\mathbf{E}(\mathbf{r},t) = E_0[\epsilon \exp[i(\mathbf{k}\cdot\mathbf{r} - \omega t)] + \text{c.c.}]/2$. In the dipole approximation, this interaction can be described by

$$V = -\mathbf{d}\cdot\mathbf{E}(\mathbf{r},t), \tag{2}$$

where $\mathbf{d}$ is the atom electric dipole. With respect to atomic parity, the operator $\mathbf{d}$ is odd, which means that this operator couples only states of opposite parities.

When the frequency ω is far from resonance and provided that the electric field is not too strong, the product of the dipole moment and the electric field is small against the detuning from the resonance, and we can apply perturbation theory. The only nonvanishing terms of the perturbation series are those of even order.

B. Second-order term in the simple case of a nondegenerate ground state

The second-order term is usually the only one which is considered. For a nondegenerate ground state g, the second-order energy shift is given by

$$U_g(\omega) = -\frac{\alpha(\omega)\langle E(t)^2\rangle}{2} = -\frac{\alpha(\omega)E_0^2}{4}, \tag{3}$$

with the polarizability $\alpha(\omega)$ given by

$$\alpha(\omega) = \frac{1}{\hbar}\sum_b \mathcal{R}e\left(\frac{|\langle b|\mathbf{d}\cdot\epsilon|g\rangle|^2}{\omega_{bg} - \omega - i\gamma_{bg}/2} + \frac{|\langle b|\mathbf{d}\cdot\epsilon|g\rangle|^2}{\omega_{bg} + \omega + i\gamma_{bg}/2}\right), \tag{4}$$

where ω_{bg} is the angular frequency of the transition from g to b and γ_{bg} the natural width of this transition. The summation also includes an integration over the ionization continuum.

C. The case of alkali atoms

In this case, it is possible to separate the contribution of the valence electron from the contribution of the inner core of the atom made of closed shells. The excitation frequencies of the inner shells are very large with respect to the laser frequency ω, and the contribution of the inner shells to the polarizability is almost independent of ω. We can write

$$\alpha(\omega) \approx \alpha_{\text{core}} + \alpha_{\text{val.}}(\omega), \tag{5}$$

where $\alpha_{\text{val.}}(\omega)$ is given by Eq. (4), the summation being limited to excited states of the valence electron.

D. Calculation of $\alpha_{\text{val.}}(\omega)$ in the presence of fine and hyperfine structure

In the presence of fine and hyperfine couplings, the atomic states are labeled by the principal quantum number n, the orbital and spin angular momenta $\mathbf{L}$ and $\mathbf{S}$, the total electronic angular momentum $\mathbf{J} = \mathbf{L} + \mathbf{S}$, the nuclear spin $\mathbf{I}$, and the total angular momentum $\mathbf{F} = \mathbf{J} + \mathbf{I}$, with the associated quantum numbers L, S, J, I, F, m_F. The dipole operator has no action on the nuclear spin and, using the Wigner-Eckart theorem, it is possible to express the valence contribution of the polarizability in the following form [26,42] (the index $val.$ is omitted to simplify the notation):

$$\alpha_{g,J,F,m_F} = \left[\alpha^{(s)}_{g,J,F} - V\cos\chi\frac{m_F}{2F}\alpha^{(v)}_{g,J,F} + \left(\frac{3\cos^2\xi - 1}{2}\right)\frac{3m_F^2 - F(F+1)}{F(2F-1)}\alpha^{(t)}_{g,J,F,}\right], \tag{6}$$

where $\alpha^{(s,v,t)}$ are the scalar, vectorial, and tensorial irreducible components of the polarizability. The orientation-dependent

coefficients are defined by the wave vector $\mathbf{k}$, the polarization vector ϵ, and the quantization axis $\mathbf{e_B} = \mathbf{B}/B$, usually defined by a static magnetic field $\mathbf{B}$. (This field is assumed to be weak enough so that the Zeeman splittings may be neglected.) We have $\cos\chi = \mathbf{k}\cdot\mathbf{e_B}$, V the fourth Stokes parameter of the light with $V\cos\chi = i(\epsilon^*\times\epsilon)\cdot\mathbf{e_B}$. $V = 1$ for right-handed and -1 for left-handed circular polarization, and $\cos\xi = \epsilon\cdot\mathbf{e_B}$. Using Eqs. (B36) and (B37) of Ref. [42], $\alpha^{(s,v,t)}$ can be written as

$$\alpha^{(s)}_{g,J,F} = \frac{1}{\sqrt{3(2F+1)}}\,\alpha^{(0)}_{g,J,F}, \quad \alpha^{(v)}_{g,J,F} = -\sqrt{\frac{2F}{(F+1)(2F+1)}}\,\alpha^{(1)}_{g,J,F}, \quad \alpha^{(t)}_{g,J,F} = -\sqrt{\frac{2F(2F-1)}{3(F+1)(2F+1)(2F+3)}}\,\alpha^{(2)}_{g,J,F}, \tag{7}$$

with

$$\alpha^{(K)}_{g,J,F} = (-1)^{K+F+1}(2F+1)\sqrt{2K+1}\sum_{n',J',F'}(-1)^{F'}(2F'+1)\begin{Bmatrix}1 & K & 1\\ F & F' & F\end{Bmatrix}\begin{Bmatrix}F & 1 & F'\\ J' & I & J\end{Bmatrix}^2\frac{|\langle n',J'||d||g,J\rangle|^2}{\hbar}$$
$$\times\,\mathcal{R}e\left(\frac{1}{\omega'-\omega-i\gamma'/2}+\frac{(-1)^K}{\omega'+\omega+i\gamma'/2}\right), \tag{8}$$

where ω' and γ' are respectively the angular frequency and the linewidth of the $g,J,F\to n',J',F'$ transition and $\langle n',J'\|d\|g,J\rangle$ is the reduced matrix element of the dipole.

E. Estimate of the first tune-out frequency for the alkali atoms

For the alkali atoms, the transitions from the ground state $^2S_{1/2}$ to the lowest in energy ^2P_J ($J = 1/2$ and $3/2$) state, i.e., the components of the D lines, have a large oscillator strength and they contribute to more than 95% of the static electric polarizability. Neglecting the hyperfine structure and the natural widths of these transitions, the contributions of these two transitions to the valence polarizability are approximately given by

$$\alpha_{\text{val.}} = \frac{1}{3\hbar}\left[\frac{d^2_{1/2}\omega_{1/2}}{\omega^2_{1/2}-\omega^2}+\frac{d^2_{3/2}\omega_{3/2}}{\omega^2_{3/2}-\omega^2}\right], \tag{9}$$

where $d_J = |\langle {}^2P_J\|d\|g,J\rangle|$ and ω_J are the dipole matrix element and frequency of the fine-structure components of the D line. In the absence of relativistic effects, these dipole moments verify $d_{3/2}\approx d_{1/2}\sqrt{2}$. In this approximation and, if the fine-structure splitting $\Delta_{FS} = \omega_{3/2}-\omega_{1/2}$ is very small with respect to $\omega_{1/2}$ and $\omega_{3/2}$ (this is particularly true for lithium), $\alpha_{\text{val.}}$ vanishes for the tune-out frequency ω_{TO} given by

$$\omega_{TO}\approx\omega_{1/2}+\frac{\Delta_{FS}}{3}. \tag{10}$$

F. Calculation of the first tune-out wavelength for lithium ^{7}Li

Lithium ^{7}Li has a nuclear spin $I = 3/2$ and thus two hyperfine ground states $F = 1$ and $F = 2$. The contribution of the core electrons to the polarizability is taken equal to the contribution $\alpha_{\text{core}} = 2.04$ a.u. to the static polarizability, as calculated by Safronova *et al.* [43]. The core contributions to the vector and tensor components are negligible, because the fine and hyperfine-structure splittings of the core excited states are very small with respect to their excitation energies.

In our experiment as well as in that of Copenhaver *et al.* [22], the laser is linearly polarized so that the vector term cancels in Eq. (6) and the tune-out frequency is measured for sublevels of the $F = 2$ level of the $^2S_{1/2}$ ground state. Dropping the irrelevant index $J = 1/2$, the valence contribution to the polarizability of these levels is given by

$$\alpha_{g,F=2,m_F} = \alpha^{(s)}_{g,F=2}+\left(\frac{3\cos^2\xi-1}{2}\right)\alpha^{(t)}_{g,F=2}\frac{m_F^2-2}{2}. \tag{11}$$

Using Eq. (8), we have calculated the irreducible components $\alpha^{(K)}_{F=2}$ of the lithium $F = 2$ hyperfine ground-state level, taking into account the excited states up to n'=7. For the $n = 2$, $J = 1/2$, $F\to n' = 2$, ^2P, J', F' transitions, we have used the reduced matrix elements of the dipole given by Safronova *et al.* [36] ($d_{1/2} = 3.3169$ a.u. and $d_{3/2} = 4.6909$ a.u.), the experimental values of the transition frequencies of Sansonetti *et al.* [44], and the transition natural width $\gamma' = 2\pi\times 5.87$ MHz measured by McAlexander *et al.* [45]. For the higher-lying states, we have used experimental values from Wiese and Fuhr [46], neglecting the natural widths γ' which are extremely small compared to the quantities $(\omega'\pm\omega)$. When the laser frequency is close to the D lines, the contribution of the higher-lying P states $n(n\geqslant 3)$ is only 0.67 au. Because of the large values of the dipole matrix elements $d_{1/2}$ and $d_{3/2}$ and the very small value of the frequency differences $(\omega'-\omega)$, comparable to the ^2P state fine structure ($\approx$10 GHz in frequency units), the contribution of the higher-lying P states shifts the tune-out frequency ν_{TO} to the red by $\approx$420 Hz only; this correction is negligible.

Figure 1 presents the polarizability $\alpha_{2,2}$ of the $F = 2$, $m_F = 2$ sublevel as a function of the laser frequency for two configurations. The first configuration is that used in our experiment, with a linear polarization ϵ perpendicular to the quantization axis $\mathbf{e_B}$, leading to $V\cos\chi = 0$ and $\xi = \pi/2$. The second configuration corresponds to a left-handed circular polarization, while the light wave vector $\mathbf{k}$ is parallel to the quantization axis $\mathbf{e_B}$, leading to $V\cos\chi = 1, \xi = \pi/2$. The shift of the tune-out frequency from the first configuration to the second one, about 3 GHz, is due to the vectorial part of the polarizability, which has a large effect in the second configuration. This result illustrates the importance of a careful alignment of the optical setup with respect to the quantization axis as well as the need of a pure laser polarization. From our calculations, we deduce the position of the tune-out frequency of the $F = 2$ level of the $^2S_{1/2}$ ground state. It is on the blue side of the $^2S_{1/2}, F = 1\to {}^2P_{1/2}, F = 1$ transition, at a

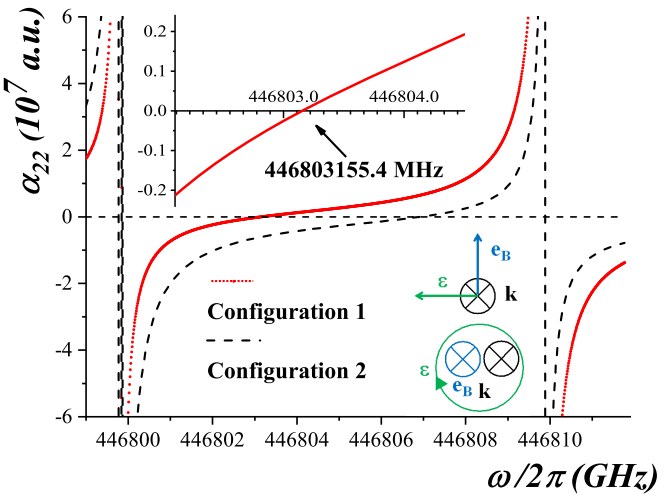

FIG. 1. Polarizability $\alpha_{2,2}$ as a function of the frequency in the region of the D_1 and D_2 lines for the two polarizations described in the text. First configuration: red bullets. Second configuration: black, dashed line. The insert zooms on the tune-out region for the first configuration.

distance (in frequency units) equal to 3384.3 ± 2.4 MHz, with a 1σ uncertainty due to the uncertainties of the dipole matrix elements $d_{1/2}$ and $d_{3/2}$.

G. Higher-order terms of the perturbation series

Up to now, we have considered only the second-order term of the perturbation series. In the case of lithium, the fine-structure splitting of the $n = 2$, ^2P state is small, $\approx$10 GHz in frequency units, and the tune-out frequency is very close to the atom resonance frequencies. With the parameters of our experiment (laser waist radius $w_0 = 61$ μm and the usual value of the laser power $P_L = 10$ mW), the value of the electric field at the center of the laser beam is $E_0 = 3.6 \times 10^4$ V/m. Using the dipole moment $d_{3/2} = 4.6909$ a.u. (i.e., $d_{3/2} \approx 4 \times 10^{-29}$ C m), we get the value of the matrix element of the perturbation $d_{3/2}E_0/h \approx 2$ GHz, which is comparable to the resonance detuning of 7 GHz. Therefore the higher orders of the perturbation theory cannot be neglected, but we have found that the fourth-order term vanishes near the tune-out frequency, and Copenhaver *et al.* [22] have shown the same property.

Finally, this calculation gives an overestimation because the atom travels through the laser beam and is not in the largest field during all its interaction with the laser beam. Moreover, we think that the beam radius was larger than the waist radius because the laser was not exactly focused on the atom interferometer arm. We have observed some nonlinear effects in laser power which are described in [47], but these effects were not very large and the shift of the tune-out frequency due to nonlinear terms is negligible.

IV. OUR EXPERIMENTAL SETUP

Our setup is implemented in our atom interferometer. In order to measure the tune-out frequency of the $F = 2, m_F = +2$ (or -2) sublevel, we optically pump the atomic beam into the chosen sublevel before it enters the interferometer. A laser beam is then focused on one interferometer arm in order to produce a phase shift of the atom fringe signal. This phase shift is measured as a function of the laser frequency and/or power. The tune-out frequency is deduced from a series of such measurements.

A. The atom interferometer

Our lithium Mach-Zehnder interferometer has been described in detail [48], and it is schematically represented in Fig. 2. The lithium atomic beam, produced by supersonic expansion of lithium seeded in argon, has a Gaussian velocity distribution with a mean velocity $v_m \approx 1050$ m/s and a 24% FWHM. This atomic beam, which is strongly collimated by two very narrow slits, crosses three laser standing waves which diffract the atom wave in the Bragg regime. We use first-order diffraction to split, reflect, and recombine the atom waves. The laser standing waves are produced by a single-frequency dye laser, with its frequency on the blue side of the $^2S_{1/2} \rightarrow {}^2P_{3/2}$ transition of ^{7}Li at 671 nm: this choice makes the interferometer very selective for this isotope, and this selectivity combined with the very large natural abundance of ^{7}Li, (92.5%) makes that only this isotope contributes to the signal [49]. This signal I is the number of atoms arriving on the Langmuir-Taylor detector during a counting period, usually $= 0.1$ s, and it is given by

$$I = I_0[1 + \mathcal{V}_{obs}\cos(\varphi_d + \varphi_P)], \tag{12}$$

where φ_d is a phase due to the diffraction process. This phase, which is independent of the atom velocity, is a function of the x position of the laser standing-wave mirrors; φ_d is used to scan the interference fringes. φ_P is a phase shift due to the perturbation under study.

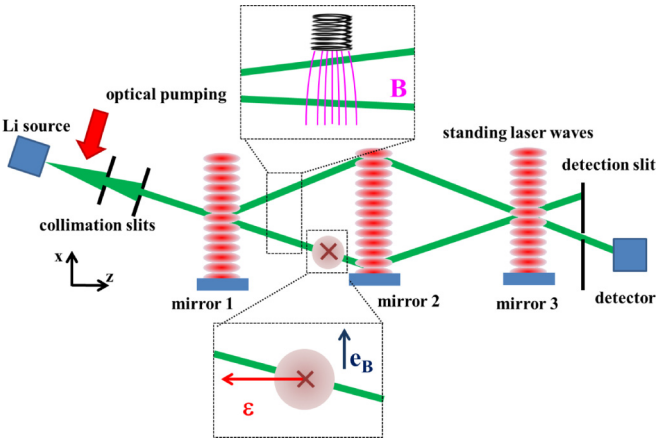

FIG. 2. Atom interferometer configuration including an optical pumping stage and a dephasing region. To measure the optical pumping efficiency, we use a coil at mid-distance between the first and second laser standing waves (upper box). This coil produces a magnetic field gradient on the interferometer arms. The lower box shows the laser interaction region. In this region, the magnetic field is along the x axis, with $B_x \approx 10^{-4}$ T. The Stark laser beam enters along the vertical y axis, perpendicular to the atom beam propagating along the z axis. This laser beam is linearly polarized with its polarization vector parallel to the z axis.

B. Stark phase shift

In order to induce a phase shift, one must apply a perturbation U on one arm and not on the other one. The best place is just ahead of the second laser standing wave, as the separation of the two interferometer arms is largest, close to 100 μm, while the FWHM of the atomic beams is about 30 μm. If the perturbation U is applied on one arm only, the phase shift φ_P, given by a semiclassical calculation, is

$$\varphi_P = -\int \frac{U}{\hbar v} dz. \tag{13}$$

This calculation is valid if U is very small with respect to the atom kinetic energy, a condition very well fulfilled. v is the atom velocity and the integral is taken along the unperturbed atom interferometer arm.

The laser beam used to produce the Stark phase shift is perpendicular to the interferometer plane and it is focused on one interferometer arm. Assuming a Gaussian TEM_{00} beam of radius w and power P_L, the Stark phase shift is equal to

$$\varphi_{S,F,m_F} = \frac{P_L}{\sqrt{2\pi}\epsilon_0 c\hbar v w}\alpha_{F,m_F}(\omega), \tag{14}$$

where c is the speed of light and ϵ_0 the vacuum permittivity. This calculation, which corresponds to the ideal case of an atom going through the center of the laser beam, neglects the fact that the other interferometer arm is also irradiated by the wing of the TEM_{00} beam. A smaller Stark phase shift is induced on this arm, and we measure their difference. This effect does not change the tune-out frequency.

C. Polarization of the laser in the interaction region

We choose to work with a linear polarization, perpendicular to the quantization axis and parallel to the atom propagation direction. A point which must be stressed is that no spin-flip occurs in the interferometer. If there is no point on the interferometer arms where the three components of the magnetic are very small at the same time, the atom angular momentum **F** follows adiabatically the direction of the magnetic field direction; this means that the projection m_F of the total angular momentum **F** on the field **B** is conserved along the atom propagation. This is why we do not control the direction of the magnetic field between the optical pumping region and the interaction region.

In the interaction region, the magnetic field **B** is made parallel to the **x** axis. For this purpose, we use two pairs of rectangular coils acting on its B_x and B_y components and a pair of circular coils acting on the B_z component. All these coils, in a quasi-Helmholtz configuration, are outside the vacuum chamber. We checked that the fringe visibility does not depend on the coil operation; this result proves that the magnetic field is sufficiently homogeneous over the interferometer arms.

D. Optical pumping of the lithium atomic beam

The optical pumping is performed before the collimation stage of the lithium atomic beam, as the random character of the photon momenta transferred to the atom would spoil the beam collimation. We have already described this optical pumping in detail [50], and we give here only an overview.

TABLE II. Relative population $P(F, m_F)$ sublevels deduced from the fits of visibility and phase-shift data. The target sublevel ($m_F = \pm 2$) is indicated on the header. In both cases, the measured efficiency of the optical pumping is very good, but a few percents of the population probably remain in the other sublevels, and the optical pumping is slightly better in the $m_F = +2$ sublevel than in the $m_F = -2$ sublevel.

Population	$m_F = +2$	$m_F = -2$
$P(2,2)$	$1.00^{+0}_{-0.04}$	$0.00^{+0.02}_{-0}$
$P(2,-2)$	$0.00^{+0.03}_{-0}$	$0.99^{+0.01}_{-0.05}$
$P(2,1)+P(1,-1)$	$0.00^{+0.02}_{-0}$	$0.01^{+0.02}_{-0}$
$P(2,-1)+P(1,1)$	$0.00^{+0.01}_{-0}$	$0.00^{+0.01}_{-0}$
$P(2,0)+P(1,0)$	$0.00^{+0.01}_{-0}$	$0.00^{+0.01}_{-0}$

In the optical pumping region, the magnetic field, controlled thanks to three pairs of square Helmholtz coils, is made parallel to the light propagation axis. We use the D_1 line because the hyperfine splittings of the $^2P_{1/2}$ state are larger than those of the $^2P_{3/2}$ state, and it is thus possible to excite more selectively the chosen hyperfine transitions. The optical pumping is produced by two circularly polarized laser beams tuned to the $^2S_{1/2},\ F = 1 \rightarrow {}^2P_{1/2},\ F' = 2$ and to the $^2S_{1/2},\ F = 2 \rightarrow {}^2P_{1/2},\ F' = 2$ transitions. The first laser beam empties the $F = 1$ level and, at the same time, modifies the m_F value, while the second one pumps the atoms into the $F = 2, m_F = \pm 2$ sublevel because this sublevel is the only one which cannot be excited. The choice of the sign of m_F of the target sublevel depends on the choice of the circular polarization for a given direction of the magnetic field.

We characterize the optical pumping efficiency by applying a magnetic field gradient on the interferometer arms (see Fig. 2). As the Zeeman phase shifts are very different for the various sublevels F, m_F, the observed atom fringe visibility and phase are functions of the sublevel populations. We measure this visibility and phase as a function of the coil current, and we extract the pumping efficiency from this measurement. Table II summarizes the relative populations of the various sublevels. These results are noticeably better than in our previous experiment [50]. The main improvement is due to a better circular polarization of the laser beams, which was obtained by replacing the vacuum windows with new ones with a lower birefringence.

E. Optical setup for the Stark laser

Figure 3 shows the optical setup which produces the Stark laser and which measures its frequency. The Stark laser beam is produced by an external cavity laser diode amplified by a tapered amplifier (Sacher TEC-420-0670-0500), and an external cavity laser diode (Toptica DL100) serves as a frequency reference. A beam from the reference laser is frequency shifted by -218 MHz using an acousto-optical modulator (AOM), and this beam is locked to the $^2S_{1/2},\ F = 1 \rightarrow {}^2P_{1/2},\ F' = 2$ transition. This frequency shift was introduced for two reasons: (i) it extends the range of measurement of the Stark laser frequency, which is limited by our spectrum analyzer, and (ii) the AOM produces sideband frequencies used for locking the frequency on a saturated absorption signal observed on a heat pipe [51].

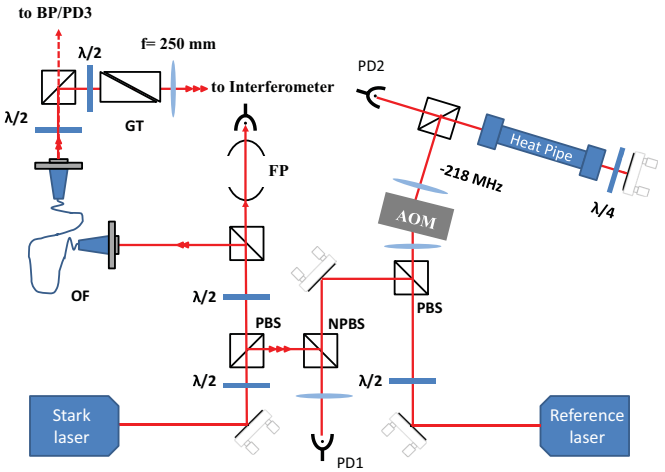

FIG. 3. Optical setup for the Stark laser. Polarizing cube beam splitters (PBSs) are used to separate the laser beams. A beam of the reference laser is frequency shifted by -218 MHz by an acousto-optic modulator (AOM) and locked on the $^2S_{1/2}$, $F = 1 \rightarrow {}^2P_{1/2}$, $F' = 2$ transition observed in a heat-pipe oven. The Stark laser frequency is locked on a resonance of a confocal Fabry-Pérot cavity. We superpose the Stark and the reference lasers by a non-polarizing beam splitter (NPBS), and the beat signal is detected by a large-bandwidth photodiode (PD1). The main beam of the Stark laser is transferred by a polarization maintaining a single mode fiber (OF) to the atom interferometer. This beam is split in two, one beam being sent to a beam profiler (BP) or a photodiode (PD3) while the other beam is focused on the interferometer arm by a 250-mm focal length lens. The polarization of this beam is cleaned by a Glan-Thompson prism (GT), and it enters the vacuum chamber though an antireflected coated window.

In order to produce an adequate lithium vapor pressure, the heat pipe is heated to 300 °C. We use two opposite windings of the Thermocoax heater with the same current to minimize the produced magnetic field and the Zeeman splittings of the transition. From the width of the transition and the error signal, we estimate the frequency stability of the reference laser to be better than 1 MHz.

A weak beam of the Stark laser is used to lock its frequency on a tunable confocal Fabry-Pérot cavity. The frequency of the Stark laser is measured by the beat note with the reference laser. The FWHM width of the beat note is smaller than 1 MHz for a 1-ms observation time. We thus get a sensitive measurement of the frequency of the Stark laser. Another weak beam of the Stark laser is used to monitor the power of the Stark laser beam; its fluctuations are smaller than 1%. The main beam of the Stark laser is transferred to the atom interferometer, using a monomode optical fiber, which also serves as a mode cleaner. This beam is enlarged by a telescope and is focused on one interferometer arm by a 250-mm-focal-length plano-convex lens. Its polarization is purified by a Glan-Thomson polarizer placed before the 250-mm focal length lens, and it enters the vacuum chamber through a high-quality AR-coated window.

We have measured the beam profile near its waist with a beam profiler (DataRay Beam'R2). The measured waist is $w_0 \approx 61$ μm, and the Rayleigh length is $L_R \approx 17$ mm. However, we have not taken into account the presence of the 10-mm-thick vacuum window. It shifts the waist further from the lens by about 3.3 mm, and the accurate height position of the interferometer arm is known with an uncertainty of the order of 3 mm. Therefore, we estimate that the offset between the waist and the interferometer arm is smaller than 7 mm.

F. Systematic effects on the frequency measurement of the Stark laser

The frequency of the reference laser is locked on the lithium transition observed by saturated absorption spectroscopy in the heat-pipe oven. Small frequency shifts may be due to the pressure shift of the lithium transition by the argon buffer gas contained in this oven (pressure below 1 mbar) or to the Zeeman effect in the local magnetic field (comparable to Earth's magnetic field). We have evaluated these effects by an experiment done before each acquisition.

We align a beam of the Stark laser in retroreflection on the mirror of the second laser standing wave. The Bragg condition insures that the surface of this mirror is parallel to the atom interferometer arms within the Bragg angle equal to ± 80 μrad. The uncertainty of this alignment is smaller than 1 mrad, which corresponds to a maximal Doppler shift of 1.4 MHz. We sweep the laser frequency near the frequency of the $^2S_{1/2}$, $F = 2 \rightarrow {}^2P_{1/2}$, $F' = 2$ transition, and the atom detector measures an intensity loss when the laser is at resonance; this intensity loss is due to the deflection of the atoms by the radiation pressure. We thus measure the frequency shift of the transition observed in the heat-pipe oven with respect to its perturbation-free position equal to 3.4 ± 1.4 MHz; the uncertainty is dominated by the laser-beam alignment.

The main Stark laser beam is introduced from the top and should be vertical. For the alignment, we used the mechanical support structure of our interferometer. The mirror mounts for the three standing laser waves are mounted on a solid aluminum bar. This bar is under the interferometer plane, and it is horizontal with a very good accuracy. Before the measurements, we place a mirror on this bar and we align the Stark laser beam by retroreflection on this mirror. We scan the frequency of this laser near resonance, and we observe the intensity loss due to photon scattering by the atoms when the laser is at resonance. We thus measure the Doppler shift equal to -11.4 ± 0.5 MHz, which corresponds to an angle of 7 mrad. During the Stark shift measurements, this mirror is replaced by another mirror which reflects the Stark laser beam out of the interferometer so that the atoms interact only once with the Stark laser beam. Due to these two effects, we estimate the uncertainty on the systematic shift of the Stark laser frequency to be equal to 2 MHz.

V. MEASUREMENT OF THE STARK PHASE SHIFT

A. Fringe signal recording and its fits

During a data acquisition period, we start by a fine tuning of the direction of the Stark laser beam using the last mirror before the $f = 250$ mm lens which is supported by a piezoelectric mirror mount. In order to maximize the overlap in the x direction of the Stark laser beam and the interferometer arm, we set the interferometric signal at midfringe, the Stark laser beam being stopped, and we observe a phase

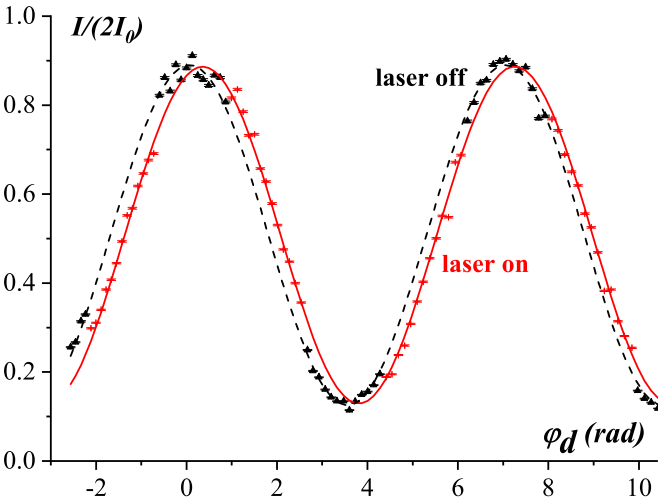

FIG. 4. Example of interferometer fringe signal $I/(2I_0)$ plotted as a function of the diffraction phase φ_d: measurements with laser off (black triangle) and their best fit (dashed black line); measurements with laser on (red crosses) and their best fit (full red line). In the present experiment, the measured value of the Stark phase shift is $\varphi_S = 213$ mrad.

shift when we apply the Stark laser beam. We then vary the direction of the Stark laser beam and we determine the position which maximizes the Stark phase shift.

To measure the Stark phase shift φ_S, we slowly scan the atom interference fringe by varying the position of the third laser standing-wave mirror and we alternate 13-s-long periods with the Stark laser beam on or off. A similar technique was used in previous studies made with our atom interferometer (e.g., [52]). Figure 4 shows such a recording and the fits of the fringe signals, from which we extract the phase shift φ_S, with a typical uncertainty near 20 mrad.

B. Determination of the tune-out frequency

We measure phase shift φ_S as a function of the Stark laser frequency. As explained above, this frequency is measured by the frequency difference Δ with the laser locked on the $^2S_{1/2}$, $F = 2 \rightarrow {}^2P_{1/2}$, $F' = 1$ transition, whose frequency is very accurately known, $446\,799\,771.121 \pm 0.013$ MHz [44]. Figure 5 displays the variation of φ_S as a function of Δ in the vicinity of the tune-out frequency, where φ_S is a linear function of Δ with a good accuracy, and a linear fit gives the frequency for which φ_S vanishes. This is the position Δ_{TO} of the tune-out frequency. In the case of Fig. 5, we get $\Delta_{TO} = 3400 \pm 1$ MHz and a slope of 1.84 ± 0.1 mrad/MHz, with 1σ uncertainty.

C. Effect due to an imperfect optical pumping

By changing the optically pumped sublevel, we have measured the Stark phase φ_S for the two $F = 2, m_F = \pm 2$ sublevels. Figure 6 presents the results of these measurements. From the linear fits, we extract the tune-out frequencies given by $\Delta_{TO}(m_F = +2) = 3407.1 \pm 0.5$ MHz and $\Delta_{TO}(m_F = -2) = 3427.4 \pm 0.6$ MHz. If the experiment was perfect, the tune-out frequency of these two sublevels should be equal,

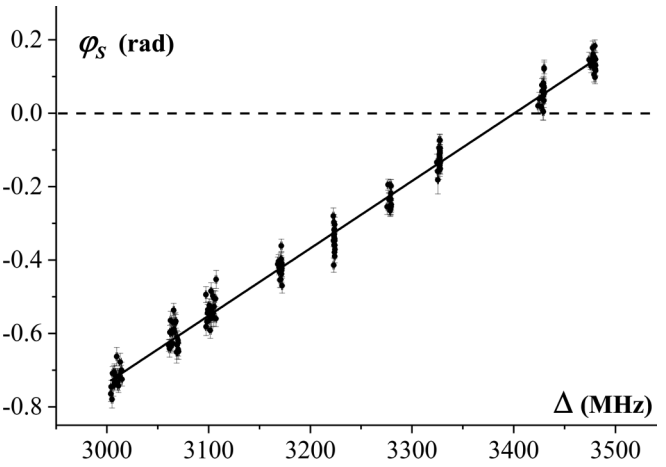

FIG. 5. Stark phase shift φ_S for the $F = 2, m_F = 2$ sublevel as a function of the frequency difference Δ: the measured phase shifts are represented by black bullets and the best linear fit by the full black line. The tune-out frequency deduced from this set of measurements corresponds to $\Delta_{TO} = (3400 \pm 1)$MHz. The laser power used for this experiment is $P_L = 10$ mW.

while we observe a frequency difference equal to 20.3 MHz. We think that this difference is due to an imperfect optical pumping, with different distributions of the population among the ground-state sublevels as shown in Table II. Using the measured distribution of the population among the ground-state sublevels and taking into account the uncertainty of the measured populations, we have calculated the possible maximum shift of the tune-out frequency thanks to Eq. (6), and this calculation confirmed our explanation.

D. Our final results

We have made eight measurements of the tune-out frequency for the $F = 2, m_F = +2$ sublevel, similar to that

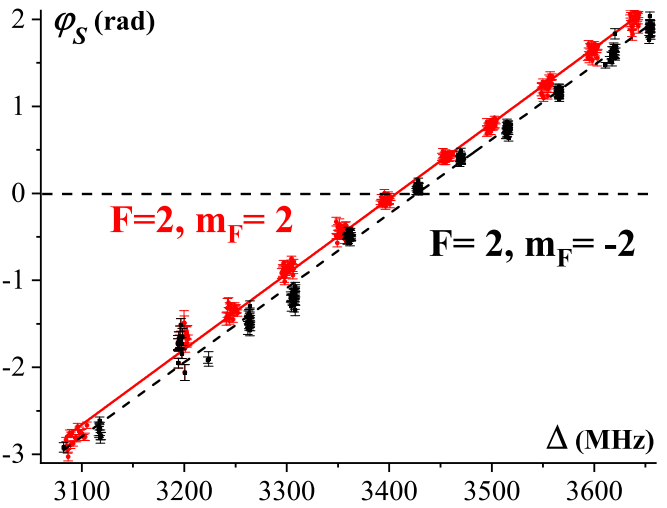

FIG. 6. Stark phase shift φ_S as a function of the frequency difference Δ. The measurements for the $F = 2$, $m_F = +2$ sublevel are represented by red bullets, those for the $F = 2$, $m_F = -2$ sublevel by black squares, and their best fits by the full (red) and dashed (black) lines, respectively. In order to increase the phase shift φ_S, the laser power used for this experiment is $P_L = 34$ mW.

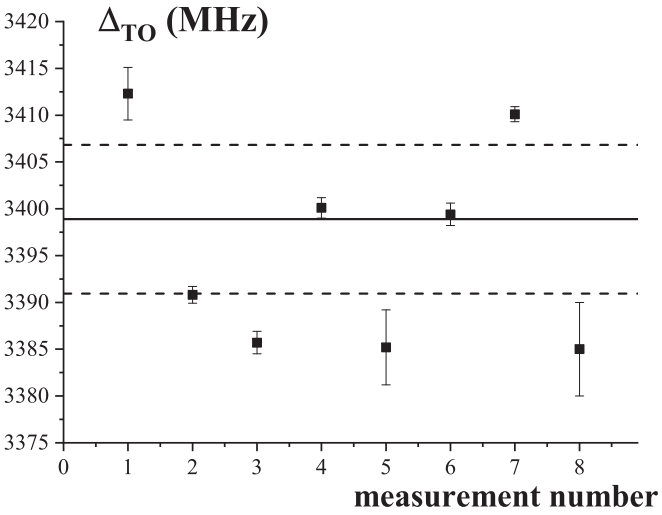

FIG. 7. Our series of measurements of the tune-out frequency Δ_{TO}. The black solid line represents their weighted mean value, and the dashed lines represent the 1σ confidence range. The large difference in the uncertainties stems from the different optical powers used.

presented in Fig. 5. Figure 7 presents the measured values of Δ_{TO}. We think that their dispersion, which is considerably larger than the uncertainties of several measurements, is due to the irreproducible character of the optical pumping. We averaged these measurements using $1/\sigma^2$ weights, and we get $\Delta_{TO} = 3399 \pm 8$ MHz. As explained above, a small Doppler shift correction, equal to -11.4 ± 0.5 MHz, must be taken into account. We thus get the corrected tune-out frequency of the $F = 2, m_F = 2$ sublevel,

$$\Delta_{TO} = 3388(8)\ \text{MHz}. \tag{15}$$

This result is in agreement with the theoretical value 3384.3 ± 2.4 MHz calculated in Sec. III. In addition to the statistical uncertainty equal to 8 MHz, a systematic uncertainty, equal to 2 MHz, is taken into account. The latter is mainly due to the uncertainty of our realization of the frequency reference. Another systematic effect is due to the broadband nonresonant light emitted by the Stark laser. This effect, calculated in the Appendix, shifts the tune-out frequency by -68 kHz, which is fully negligible.

E. Comparison with the results of Copenhaver *et al.* [22]

Let us compare our measurement with that of Copenhaver *et al.* [22]. Both experiments have measured the tune-out frequency at 671 nm of ^{7}Li, but the two experimental setups are very different in many aspects. The most important differences are as follows:

(i) The interaction time with the Stark laser is considerably larger in their experiment, so they need a smaller power density.

(ii) The atom interferometer selectivity in F, m_F is different, which is obtained by a combination of optical pumping and destruction of the coherence of a complementary interferometer.

TABLE III. Values of the tune-out frequency of the scalar polarizability obtained by theory or by experiment. For our measurement, we give two values corresponding to two values of $3A/(4\pi)$ due to the tensorial polarizability. We took either the experimental value of [22] (56.9 MHz) or the theoretical value (47 MHz). These four values of $\Delta_{TO,s}$ are in good agreement.

Method	$3A/(4\pi)$ MHz	$\Delta_{TO,s}/(2\pi)$ (MHz)
Experiment [22]	56.9 ± 4.7 [22]	3310.6 ± 4.9
Our experiment	56.9 ± 4.7 [22]	3315 ± 8
Our experiment	47 (Theory)	3312 ± 8
Theory	47 (Theory)	3308.1 ± 2.4

(iii) They measured the tune-out frequency of the $F = 2, m_F = 0$ sublevel, and they measured the variation of this frequency with the angle ξ between the laser polarization and the quantization axis.

(iv) They use as a reference frequency the $^2S_{1/2}, F = 2 \rightarrow {}^2P_{1/2}, F' = 2$ transition, which differs from our reference frequency corresponding to the $^2S_{1/2}, F = 2 \rightarrow {}^2P_{1/2}, F' = 1$ transition by the hyperfine splitting of the $^2P_{1/2}$ level equal to 91.9 MHz [56].

To compare our result to the result of Ref. [22], we first subtract this hyperfine splitting from our value of Δ_{TO} to take the same reference, and we get $\Delta_{TO}^{(corr.)} = 3296(8)$ MHz. We must also take into account the different contributions of the tensor polarizability, as we used different sublevels. Finally, as discussed by various papers, it is traditional to define the tune-out frequency $\omega_{TO,s}(F)$ as the frequency for which the scalar polarizability vanishes, $\alpha^{(s)}(F, \omega_{TO,s}) = 0$. Equation (11) gives the variation of $\alpha_{F=2,m_F}$ with m_F and with the angle ξ. A first-order Taylor expansion of Eq. (11) around the tune-out frequency $\omega_{TO,s}$ gives the dependence of $\omega_{TO}(F, m_F, \xi)$ on m_F and ξ:

$$\omega_{TO}(F, m_F, \xi) \approx \omega_{TO,s} - A\frac{3\cos^2\xi - 1}{2} \times \frac{m_F^2 - 2}{2}$$
$$\text{with } A \approx \frac{\alpha^{(t)}(\omega)}{d\alpha(\omega)/d\omega} \text{ for } \omega = \omega_{TO,s}. \tag{16}$$

The range covered by $\omega_{TO}(F, m_F, \xi)$ when ξ varies from 0 to $\pi/2$ is $3A/2$. The measurement by Copenhaver *et al.* [22] gives $3A/(4\pi) = 56.9 \pm 4.7$ MHz, while theory predicts $3A/(4\pi) = 47$ MHz. Using these two values, we can deduce the difference $\Delta_{TO,s}$ between the frequency $\omega_{TO,s}$ and the frequency of the $^2S_{1/2}, F = 2 \rightarrow {}^2P_{1/2}, F' = 2$ transition. These experimental values, as well the theoretical value of $\Delta_{TO,s}$, are collected in Table III.

F. Information on the oscillator strengths of the *D*1 and *D*2 lines

As explained in Sec. III, the tune-out frequency is very sensitive to the ratio R of the dipole matrix elements squared of the D_1 and D_2 lines,

$$R = d_{3/2}^2/d_{1/2}^2. \tag{17}$$

In Sec. III F, we calculated the theoretical tune-out frequency. For this calculation we used the reduced matrix elements of the dipole given by Safronova *et al.* [36] [see Eq. (6)].

TABLE IV. Experimental values of the ratio $R = d_{3/2}^2/d_{1/2}^2$ of the squared dipole matrix elements of the components of the D lines of alkali atoms.

Atom	Ratio	Method	Ref.
^{7}Li	1.999(7)	Atom interferometry	Present work
^{7}Li	2.001(4)	Atom interferometry	[22]
^{23}Na	1.9994(37)	Spectroscopy	[14,53]
K	1.9977(11)	Atom interferometry	[25]
^{87}Rb	1.99219(3)	Atom interferometry	[26]
Cs	1.9809(9)	Spectroscopy	[54]
^{210}Fr	1.9011(11)	Spectroscopy	[55]

As the tune-out frequency depends on the exact value of R, we have fitted R in order to match our measurement of the tune-out frequency value and we get $R = 1.999(7)$. The given uncertainty comes from the statistical (7) and the systematic one (1).

Using the measurement of Copenhaver *et al.* [22], we get $R = 2.001(4)$. The calculations of Tang *et al.* [37] use $R - 2 = 0.000\,024\,107$, quoting an unpublished relativistic calculation due to Jiang. A test of the value of R at the 10^{-5} level requires reducing the uncertainty on the tune-out frequency to near 10 kHz. We have collected the experimental values of the ratio R for the first resonance line of alkali atoms (see Table IV). R differs from the value $R = 2$, and this deviation increases rapidly with the nuclear charge Z because of relativistic effects.

VI. CONCLUSION

This paper describes the measurement of the tune-out frequency of ^{7}Li at 671 nm between the $D1$ and $D2$ lines. For this measurement, we used our atom interferometer with the atoms optically pumped in the $F = 2$, $m_F = +2$ (or -2) sublevel. One arm of the interferometer was irradiated by a laser beam, and we measured the phase shift due to the dynamical Stark effect as a function of the laser frequency. This frequency was measured by comparing the Stark laser and a reference laser locked on the frequency of the $^2S_{1/2}$, $F = 1 \rightarrow {}^2P_{1/2}$, $F' = 2$ transition. Although the achieved optical pumping was very good, we found that the main uncertainty on the measurement of the tune-out frequency is due to the presence of a few percent of the atoms left in other sublevels than in the target sublevel.

This defect is not stable in time, and the eight individual measurements of the tune-out frequency of the $F = 2$, $m_F = +2$ sublevel present some dispersion; because of this dispersion, our final uncertainty on this frequency is 8 MHz. Its value is in very good agreement with our calculation using the dipole moments of Safronova *et al.* [36], including the effect of hyperfine structure. Our measurement is also in very good agreement with the measurement of Copenhaver *et al.* [22], after correction for the different contributions of the tensorial term.

Our final value of the tune-out frequency of the scalar polarizability is

$$\omega_{TO,s}/(2\pi) = 446\,803\,175(8)\ \text{MHz}, \tag{18}$$

where we have used the theoretical value of the tensorial term. The uncertainty of 8 MHz comes from the statistical (8 MHz) and the systematic one (2 MHz). The corresponding tune-out wavelength is 670 972 085(11) fm (11 fm statistical and 3 fm systematic). We have interpreted our measurement in terms of the ratio of the oscillator strengths of the components of the D line, and we find that $R = d_{3/2}^2/d_{1/2}^2 = 1.999(7)$. This result is in agreement with a recent calculation [37] which is extremely precise.

ACKNOWLEDGMENTS

Many thanks to the technical and administrative staffs of our laboratory for their help. We thank A. Cronin, C. Meier, T. Saue, and T. Fleig for fruitful discussions. Special thanks go to E. Michon for his participation to an early stage of this experiment. Financial support from Centre National de la Recherche Scientifique (CNRS) INP, ANR (Grant No. ANR-11-BS04-016: HIPATI), and Université Toulouse III – Paul Sabatier is gratefully acknowledged.

APPENDIX: INFLUENCE OF BACKGROUND LIGHT EMITTED BY THE STARK LASER SYSTEM

The Stark laser is a tapered laser diode which emits, in addition to the laser line, a broad background. This background light produces a supplementary phase shift φ_{bg} of the atom wave, and this phase shift must be taken into account for the measurement of the tune-out frequency. To describe the spectrum of this background, we used the data sheet of our laser system given by the manufacturer (Sacher Lasertechnik GmbH) [57]. This data sheet describes the spectrum as a broad component and a Gaussian peak corresponding to the laser line, the width of the Gaussian peak being limited by the resolution of the spectrometer. We use a modified Gaussian-like

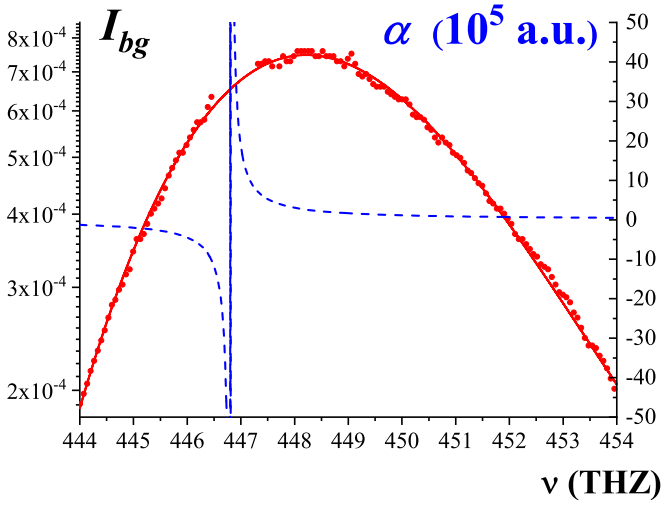

FIG. 8. Plot of the spectrum $I_{bg}(\nu)$ of the background light emitted by our amplified laser system as a function of the light frequency ν. The data points (red bullets) are from the Sacher Lasertechnik data sheet (the laser peak has not been represented), provided by [57], and their fit (red full line) (left scale). Lithium polarizability $\alpha(\omega)$ with $\omega = 2\pi\nu$ approximately given by Eq. (9) also represented by the blue dashed line (right scale).

equation to fit the intensity I_{bg} if the background spectrum

$$I_{bg}(\nu) = I_{0,dg} \exp\left(- \frac{(\nu - \nu_{bg})^2}{\Delta\nu_{bg}^2} + a_3(\nu - \nu_{bg})^3 \right). \quad \text{(A1)}$$

This spectrum and its fit are represented in Fig. 8. The parameters given by the fit are $\nu_{bg} = (448.22 \pm 0.01)$ THz, $\Delta\nu_{bg} = (4.03 \pm 0.01)$ THz, and $a_3 = (3.94 \pm 0.08) \times 10^{-3}$ THz^{-3}. From the data sheet, we have also calculated the ratio of the power P_L of the laser line and the power P_{bg} of the background, and we have found $P_{bg}/P_L = 5.3 \times 10^{-3}$.

We can now calculate the Stark phase shift due to the background light. We have done this calculation using the polarizability $\alpha(\omega)$ given by Eq. (9), which neglects hyperfine structure. This calculation involves the integral $\int I_{bg}[\omega/(2\pi)]\alpha(\omega)d\omega$, which has two singularities for $\omega = \omega_{1/2}$ and $\omega_{3/2}$. We calculate the principal values numerically with MATHEMATICA [58]. Our final result is that, for the laser power $P_L = 10$ mW used for our measurements, the tune-out frequency is shifted by -20 kHz, which is negligible with respect to our experimental uncertainty.

[1] *Atom Interferometry*, edited by P. R. Berman (Academic Press, New York, 1997).

[2] A. D. Cronin, J. Schmiedmayer, and D. E. Pritchard, Rev. Mod. Phys. **81**, 1051 (2009).

[3] *Atom Interferometry, Proceedings of the International School of Physics Enrico Fermi*, edited by G. M. Tino and M. A. Kasevich (IOS Press, Amsterdam, 2014), Vol. 188.

[4] H. Scheffers and J. Stark, Phys. Z. **35**, 625 (1934).

[5] K. D. Bonin and V. V. Kresin, *Electric-Dipole Polarizabilities of Atoms, Molecules and Clusters* (World Scientific, Singapore, 1997).

[6] J. Mitroy, M. S. Safronova, and C. W. Clark, J. Phys. B **43**, 202001 (2010).

[7] C. R. Ekstrom, J. Schmiedmayer, M. S. Chapman, T. D. Hammond, and D. E. Pritchard, Phys. Rev. A **51**, 3883 (1995).

[8] T. D. Roberts, A. D. Cronin, M. V. Tiberg, and D. E. Pritchard, Phys. Rev. Lett. **92**, 060405 (2004).

[9] A. Miffre, M. Jacquey, M. Büchner, G. Trénec, and J. Vigué, Phys. Rev. A **73**, 011603(R) (2006).

[10] A. Miffre, M. Jacquey, M. Büchner, G. Trénec, and J. Vigué, Eur. Phys. J. D **38**, 353 (2006).

[11] B. Deissler, K. J. Hughes, J. H. T. Burke, and C. A. Sackett, Phys. Rev. A **77**, 031604(R) (2008).

[12] W. F. Holmgren, M. C. Revelle, V. P. A. Lonij, and A. D. Cronin, Phys. Rev. A **81**, 053607 (2010).

[13] M. D. Gregoire, I. Hromada, W. F. Holmgren, R. Trubko, and A. D. Cronin, Phys. Rev. A **92**, 052513 (2015).

[14] M. D. Gregoire, N. Brooks, R. Trubko, and A. D. Cronin, Atoms **4**, 21 (2016).

[15] P. Massignan and Y. Castin, Phys. Rev. A **74**, 013616 (2006).

[16] L. J. LeBlanc and J. H. Thywissen, Phys. Rev. A **75**, 053612 (2007).

[17] B. Arora, M. S. Safronova, and C. W. Clark, Phys. Rev. A **84**, 043401 (2011).

[18] J. Catani, G. Barontini, G. Lamporesi, F. Rabatti, G. Thalhammer, F. Minardi, S. Stringari, and M. Inguscio, Phys. Rev. Lett. **103**, 140401 (2009).

[19] G. Lamporesi, J. Catani, G. Barontini, Y. Nishida, M. Inguscio, and F. Minardi, Phys. Rev. Lett. **104**, 153202 (2010).

[20] M. S. Safronova, Z. Zuhrianda, U. I. Safronova, and C. W. Clark, Phys. Rev. A **92**, 040501(R) (2015).

[21] B. M. Henson, R. I. Khakimov, R. G. Dall, K. G. H. Baldwin, L. Y. Tang, and A. G. Truscott, Phys. Rev. Lett. **115**, 043004 (2015).

[22] E. Copenhaver, K. Cassella, R. Berghaus, and H. Müller, Phys. Rev. A **100**, 063603 (2019).

[23] W. F. Holmgren, R. Trubko, I. Hromada, and A. D. Cronin, Phys. Rev. Lett. **109**, 243004 (2012).

[24] R. Trubko, J. Greenberg, M. T. St. Germaine, M. D. Gregoire, W. F. Holmgren, I. Hromada, and A. D. Cronin, Phys. Rev. Lett. **114**, 140404 (2015).

[25] R. Trubko, M. D. Gregoire, W. F. Holmgren, and A. D. Cronin, Phys. Rev. A **95**, 052507 (2017).

[26] R. H. Leonard, A. J. Fallon, C. A. Sackett, and M. S. Safronova, Phys. Rev. A **92**, 052501 (2015); **95**, 059901(E) (2017).

[27] F. Schmidt, D. Mayer, M. Hohmann, T. Lausch, F. Kindermann, and A. Widera, Phys. Rev. A **93**, 022507 (2016).

[28] H. Xia, C. O'Brien, S. Suckewer, and M. O. Scully, Phys. Rev. A **93**, 053810 (2016).

[29] C. D. Herold, V. D. Vaidya, X. Li, S. L. Rolston, J. V. Porto, and M. S. Safronova, Phys. Rev. Lett. **109**, 243003 (2012).

[30] W. Kao, Y. Tang, N. Q. Burdick, and B. L. Lev, Opt. Express **25**, 3411 (2017).

[31] J. Mitroy and L.-Y. Tang, Phys. Rev. A **88**, 052515 (2013).

[32] R. P. M. J. W. Notermans, R. J. Rengelink, K. A. H. van Leeuwen, and W. Vassen, Phys. Rev. A **90**, 052508 (2014).

[33] Y.-H. Zhang, L.-Y. Tang, X.-Z. Zhang, and T.-Y. Shi, Phys. Rev. A **93**, 052516 (2016).

[34] G. W. F. Drake, J. G. Manalo, P.-P. Zhang, and K. G. H. Baldwin, Hyperfine Interact. **240**, 31 (2019).

[35] Y.-H. Zhang, F.-F. Wu, P.-P. Zhang, L.-Y. Tang, J.-Y. Zhang, K. G. H. Baldwin, and T.-Y. Shi, Phys. Rev. A **99**, 040502(R) (2019).

[36] M. S. Safronova, U. I. Safronova, and C. W. Clark, Phys. Rev. A **86**, 042505 (2012).

[37] L.-Y. Tang, M. W. J. Bromley, Z.-C. Yan, and J. Mitroy, Phys. Rev. A **87**, 032507 (2013).

[38] J. Jiang, L.-Y. Tang, and J. Mitroy, Phys. Rev. A **87**, 032518 (2013).

[39] U. Dammalapati, K. Harada, and Y. Sakemi, Phys. Rev. A **93**, 043407 (2016).

[40] S. Singh, B. K. Sahoo, and B. Arora, Phys. Rev. A **94**, 023418 (2016).

[41] Y. Cheng, J. Jiang, and J. Mitroy, Phys. Rev. A **88**, 022511 (2013).

[42] F. L. Kien, P. Schneeweiss, and A. Rauschenbeutel, Eur. Phys. J. D **67**, 92 (2013).

[43] M. S. Safronova, B. Arora, and C. W. Clark, Phys. Rev. A **73**, 022505 (2006).

[44] C. J. Sansonetti, C. E. Simien, J. D. Gillaspy, J. N. Tan, S. M. Brewer, R. C. Brown, S. Wu, J. V. Porto *et al.*, Phys. Rev. Lett. **107**, 023001 (2011).

[45] W. I. McAlexander, E. R. I. Abraham, and R. G. Hulet, Phys. Rev. A **54**, R5 (1996).
[46] W. L. Wiese and J. R. Fuhr, J. Phys. Chem. Ref. Data **38**, 565 (2009).
[47] B. Decamps, Ph.D. thesis, Université Paul Sabatier, 2017, https://tel.archives-ouvertes.fr/tel-01447591v1.
[48] A. Miffre, M. Jacquey, M. Büchner, G. Trénec, and J. Vigué, Eur. Phys. J. D **33**, 99 (2005).
[49] M. Jacquey, A. Miffre, M. Büchner, G. Trénec, and J. Vigué, Eur. Phys. Lett. D **77**, 20007 (2007).
[50] J. Gillot, A. Gauguet, M. Büchner, and J. Vigué, Eur. Phys. J. D **67**, 263 (2013).
[51] J. Gillot, C. Lemarchand, I. Braud, B. Decamps, A. Gauguet, J. Vigué, and M. Büchner, Rev. Sci. Instrum. **84**, 106109 (2013).
[52] S. Lepoutre, A. Gauguet, G. Trénec, M. Büchner, and J. Vigué, Phys. Rev. Lett. **109**, 120404 (2012).
[53] U. Volz and H. Schmoranzer, Phys. Scr. **T65**, 48 (1996).
[54] R. J. Rafac and C. E. Tanner, Phys. Rev. A **58**, 1087 (1998).
[55] J. E. Simsarian, L. A. Orozco, G. D. Sprouse, and W. Z. Zhao, Phys. Rev. A **57**, 2448 (1998).
[56] Y.-C. Huang, W.-J. Luo, Y.-T. Kuo, and L.-B. Wang, J. Phys. B **46**, 075004 (2013).
[57] Sacher GmbH, private communication of data sheets for TEC-420-0670-0500 laser.
[58] Wolfram Research, MATHEMATICA version 11.1.1.